

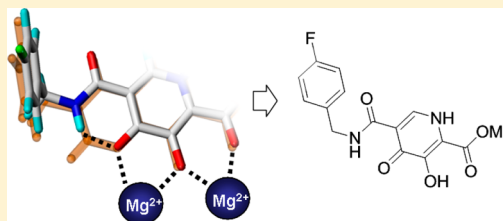
# Carbamoyl Pyridone HIV-1 Integrase Inhibitors. 1. Molecular Design and Establishment of an Advanced Two-Metal Binding Pharmacophore

Takashi Kawasaki,<sup>\*,†</sup> Brian A. Johns,<sup>‡</sup> Hiroshi Yoshida,<sup>†</sup> Teruhiko Taishi,<sup>†</sup> Yoshiyuki Taoda,<sup>†</sup> Hitoshi Murai,<sup>†</sup> Ryuichi Kiyama,<sup>†</sup> Masahiro Fuji,<sup>†</sup> Tomokazu Yoshinaga,<sup>†</sup> Takahiro Seki,<sup>†</sup> Masanori Kobayashi,<sup>†</sup> Akihiko Sato,<sup>†</sup> and Tamio Fujiwara<sup>†</sup>

<sup>†</sup>Shionogi Pharmaceutical Research Center, Shionogi & Co., Ltd., 3-1-1 Futaba-cho, Toyonaka-shi, Osaka 561-0825, Japan

<sup>‡</sup>GlaxoSmithKline Research & Development, Infectious Diseases Therapeutic Area Unit, Five Moore Drive, Research Triangle Park, North Carolina 27709, United States

**ABSTRACT:** Our group has focused on expanding the scope of a two-metal binding pharmacophore concept to explore HIV-1 integrase inhibitors through medicinal chemistry efforts to design novel scaffolds which allow for improvement of pharmacokinetic (PK) and resistance profiles. A novel chelating scaffold was rationally designed to effectively coordinate two magnesium cofactors and to extend an aromatic group into an optimal hydrophobic pharmacophore space. The new chemotype, consisting of a carbamoyl pyridone core unit, shows high inhibitory potency in both enzymatic and antiviral assay formats with low nM IC<sub>50</sub> and encouraging potency shift effects in the presence of relevant serum proteins. The new inhibitor design displayed a remarkable PK profile suggestive of once daily dosing without the need for a PK booster as demonstrated by robust drug concentrations at 24 h after oral dosing in rats, dogs, and cynomolgus monkeys.



## 1. INTRODUCTION

Anti-HIV drugs are categorized based on their inhibitory mechanism with the most prominent targeting virally encoded enzymatic machinery in the following classes: nucleoside reverse transcriptase inhibitors (NRTIs), non-nucleoside reverse transcriptase inhibitors (NNRTIs), protease inhibitors (PIs), and integrase inhibitors (INIs). Combination therapy using the above classes of inhibitors called highly active antiretroviral therapy (HAART) has been successful in effective HIV/AIDS treatment.<sup>1</sup> Integrase (IN) is a virally encoded enzyme essential for retrovirus replication that catalyzes the integration of viral DNA into the host cell DNA. As a result of this unique step in the retroviral life cycle, integrase has become an attractive target for drug discovery. The integration process promoted by IN consists of two sequential reactions.<sup>2</sup> In the first step, HIV-1 IN removes a dinucleotide from each end of the viral DNA, generating two CA-3' hydroxyl recessed termini. The next step is a transesterification reaction of the newly formed 3' hydroxyl groups attacking the phosphodiester backbone of the host DNA. Subsequent cell repair mechanisms are implicated during completion of the viral DNA integration. Both reactions are catalyzed by the highly conserved catalytic core of HIV-1 IN which consists of two divalent metal ions held in place by a DD(35)E triad of protein carboxylate side chains (Asp64, Asp116, and Glu152). The two-metal binding pharmacophore model<sup>3</sup> has been of great utility as a platform for inhibitor design as graphically depicted in Figure 1a. In its most simplified format, the concept involves a drug molecule

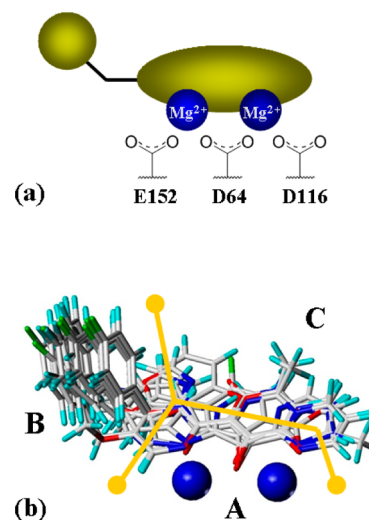


**Figure 1.** (a) Graphical depiction of the two-metal binding pharmacophore. (b) Structural overlapping model of many historical two-metal binding scaffolds. Yellow lines partition the structures into each pharmacophore regions A, B, and C.

chelating both metal cofactors, which for HIV-1 IN have been shown to be Mg<sup>2+</sup> in the active site of the enzyme to prevent

Received: July 17, 2012

Published: September 10, 2012

catalysis and stabilization of the transesterification intermediate involving the host DNA phosphodiester group. Moreover, the minimal pharmacophore should contain an aromatic group extend into an adjacent hydrophobic space. Continuous efforts have been directed toward the discovery of small molecule inhibitors over the past decade based on the two metal binding pharmacophore concept.<sup>4</sup> These efforts have culminated in the discovery of raltegravir (RAL), the first marketed HIV-1 integrase inhibitor (Figure 2).<sup>5</sup> RAL is becoming the preferred

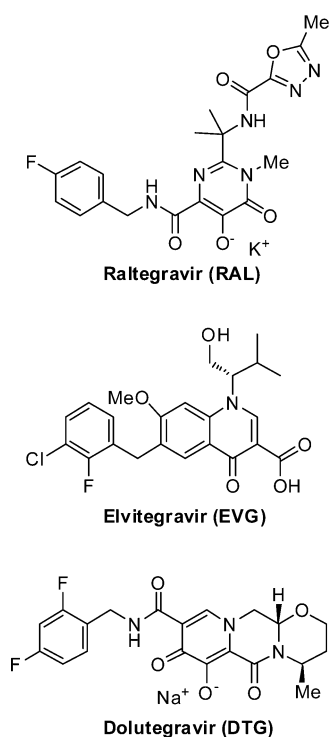


Figure 2. HIV-1 integrase inhibitors.

third agent in many HAART regimens for both treatment naive and experienced patients.<sup>6</sup> RAL requires a 400 mg twice daily dose and has given rise to clear signature mutation pathways (N155H, Q148H/K/R, and Y143C/R).<sup>7</sup> As a result there are significant remaining issues to be improved including overall dose burden, dosing interval, potency against resistant mutations, and genetic barrier to resistance. Elvitegravir<sup>8</sup> (EVG) is another first generation INI which is currently under NDA review. EVG allows for a once daily dose of 150 mg, however, this requires coadministration of a CYP3A inhibitor as a PK booster.<sup>9</sup> Additionally, EVG has significant cross resistance with RAL.<sup>10</sup>

Since the diketo acid (DKA) series were identified,<sup>11</sup> our group has pursued medicinal chemistry efforts using a two-metal binding pharmacophore structural based design. These efforts included extensive study of three early generations of INIs consisting of hydroxyquinoline (OXN), hydroxynaphthyridine (NAP), and hydroxynaphthyridinone (NTD) core chelating motifs (Figure 3).<sup>12</sup> However, all of these efforts along with a multitude of contributions from other groups ultimately fell short of delivering necessary advancements required to provide true differentiation for patients in the areas where RAL and EVG have demonstrated limitations. We wish to report herein molecular design methodology around a series of carbamoyl pyridone integrase inhibitors that utilize a novel

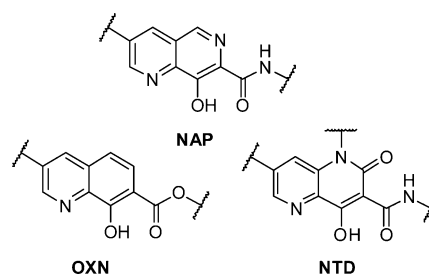


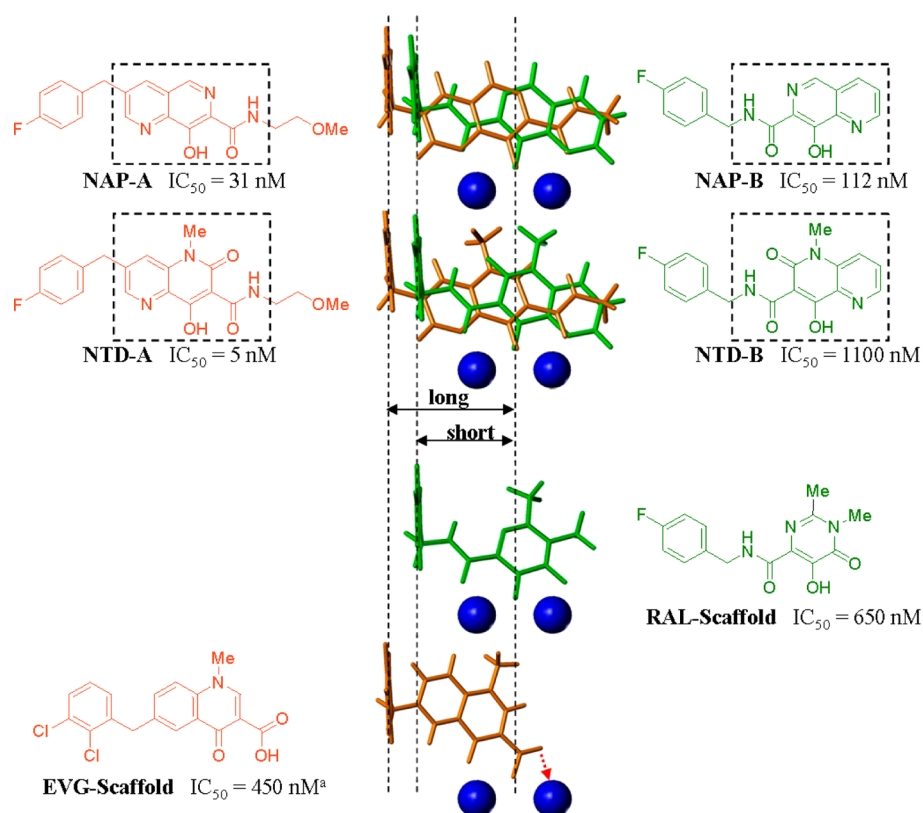
Figure 3. Early generations of two-metal binding scaffolds hydroxyquinoline (OXN), hydroxynaphthyridine (NAP), and hydroxynaphthyridinone (NTD).

two-metal binding motif as a first step toward differentiation of an INI to begin to address the above issues limiting RAL and EVG. These results are the first installment of a series of reports that lead to the discovery of the next generation INI dolutegravir (DTG), which is currently in late clinical trial evaluation as an unboosted, low dose once daily INI with superior resistance profile.

## 2. MOLECULAR DESIGN

A structural overlapping model of many historical two-metal binding scaffolds is shown in Figure 1b. This model has more recently been validated by the elegant crystallography studies by Cherepanov using the prototype foamy virus integrase system as a homologue of the HIV-1 protein.<sup>13</sup> Region A is the two-metal binding motif critical to all members of this class of strand transfer active site binders. Region B is a hydrophobic region stemming from extensive historical SAR from our laboratories and others that requires a substituted benzyl group and does not appear tolerant of significant departures from this motif.<sup>4</sup> Region C is commonly quite flexible and tolerable to structural modifications to allow for optimization of the PK and other drug-like properties required of an orally dosed small molecule. There is also evidence that region C enhances antiviral potency although the structure–activity relationship and tolerance to variation is less strict than regions A and B.<sup>8</sup>

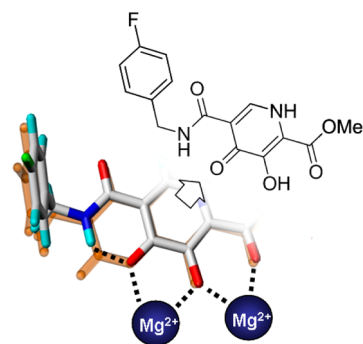
Our molecular design study began with a focus on region B. Phenyl rings are clustered as indicated in Figure 1b, however, upon closer inspection there appeared to be a range of space occupied by the different rings with an associated impact on potency. Figure 4 shows a comparison of several examples with varied spacing of the region B hydrophobic benzyl group. Both NAP-A and NAP-B have an identical 8-hydroxynaphthyridine metal chelation motif but are effectively rotated on a pseudo C<sub>2</sub> symmetry axis by placing the benzyl group on opposite ends of the heterocycle. As such the NAP-A and NAP-B scaffolds are proposed to bind in a reversed orientation to one another, thereby placing the hydrophobic benzyl group in the same pharmacophore space. When the two molecules were overlapped based on the metal binding region as shown in the middle, there is a small but clear difference in the location of the phenyl ring. The situation is similar for the naphthyridinones NTD-A and -B.<sup>12</sup> Again, the hydrophobic region of NTD-A is further extended than that of NTD-B. It should be noticed that the longer spacing of the type NAP-A and NTD-A consistently show higher potency.<sup>12</sup> Interestingly a simplified RAL-scaffold shown in Figure 4, which has a short benzyl group spacing, has only weak to modest antiviral potency, but by additional modifications to region C RAL is able to achieve low nM potency.<sup>5</sup> On the contrary, the EVG quinolone scaffold



**Figure 4.** Comparison of hydrophobic region spacing effects on antiviral efficacies. Other data are from internal experiments.<sup>12</sup> <sup>a</sup>Data reported in ref 8.

contains an extended phenyl group similar to the NAP-A and NTD-A structures. However, metal chelation could not be optimally completed due to weak 1–3-bidentate coordination by the carboxylic acid unit. Again, by additional modifications to the quinolone carboxylic acid scaffold, EVG achieved high potency.<sup>8</sup> The above small data set of aromatic spacing differences leading to potency improvements is further supported by many similar observations in our hands with other scaffolds not reported herein and has served as a basis for evolution of our model to refine a preferable placement of the hydrophobic region B.

As a next step, we focused on the metal chelation properties of the three scaffolds which consistently contain a nitrogen–oxygen–oxygen chelating unit. As is generally accepted, integrase uses divalent magnesium cofactors under physiological conditions.<sup>11,14</sup> According to the hard and soft acid and base (HSAB) theory, ionic magnesium is categorized as hard metal, therefore a hard base, such as oxygen is preferred over nitrogen to coordinate a magnesium metal in the active site. As such, replacement of the nitrogen in NTD-A with oxygen in the chelation unit was proposed. An additional benefit with using a harder base, such as oxygen, is to reduce potential side effects caused by nonspecific binding to soft metals utilized in other biological functions in the human body. Our first attempt at replacement of the nitrogen with an oxygen is shown in Figure 5. Because of bonding differences in an oxygen versus a nitrogen, the ring system in the NAP and NTD scaffolds was opened to utilize an “acyclic” carbonyl as the Lewis basic chelation group. The prior scaffold “ring” integrity and positioning of the benzyl group was maintained by placement of a carboxamide in the 5-position of the pyridone system whereby an intramolecular hydrogen bonding with the

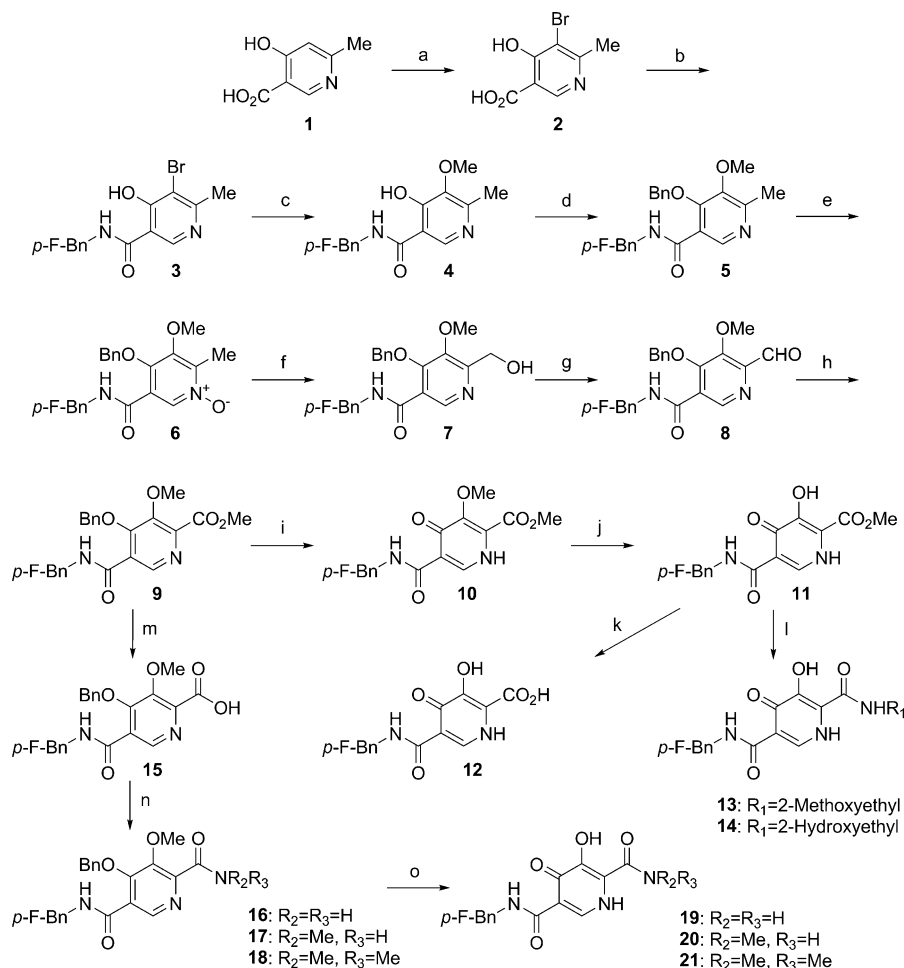


**Figure 5.** Carbamoyl pyridone scaffold design. Orange stick represents a pyridine containing skeleton of the OXN, NAP, or NTD scaffold. A stick model colored by atom type represents the new carbamoyl pyridone containing scaffold. An intramolecular hydrogen bonding and two distinct metal chelations interactions are represented by dotted black lines.

pyridone core carbonyl allowed for coplanarity and re-establishment of the original scaffold pseudoring system. With this design, the benzyl is placed in the desired hydrophobic pharmacophore region, thereby maintaining a favorable region B alignment. In this paper, we report antiviral efficacies against not only wild type but also some of key resistant variants as well as initial animal PK profiles that serve to validate this first step in rationally designing a next generation INI.

### 3. CHEMISTRY

All final compounds were prepared from the key protected intermediate **9** upon the appropriate synthetic manipulations (Scheme 1). The intermediate **9** was prepared as follows. After

Scheme 1. Synthesis of Compounds<sup>a</sup>

<sup>a</sup>Reagents and conditions: (a) bromine, acetic acid–water, 65 °C; (b) 4-fluorobenzylamine, HOBT, 1-ethyl-3-(3-dimethylaminopropyl)carbodiimide hydrochloride, DMF, rt; (c) NaOMe, methanol–DMF, 105 °C; (d) BnOH, *n*-Bu<sub>3</sub>P, DIAD, THF, reflux; (e) *m*-CPBA, chloroform, rt; (f) Ac<sub>2</sub>O, 80 °C; (g) SO<sub>3</sub>–pyridine, Et<sub>3</sub>N, DMSO, chloroform, rt; (h) KOH, iodine, methanol, rt; (i) TMSCl, NaI, acetonitrile, 0 °C; (j) AlCl<sub>3</sub>, chloroform, rt; (k) LiOH, methanol–water, 60 °C; (l) amine, methanol, microwave, 140 °C; (m) NaOH, methanol–water, rt; (n) HOBT, 1-ethyl-3-(3-dimethylaminopropyl)carbodiimide hydrochloride, amine, DMF, rt; (o) pyridine–HCl, 180 °C.

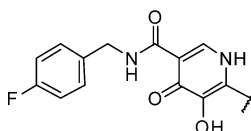
bromination of commercially available 4-hydroxy-6-methylnicotinic acid **1**, amidation with 4-fluorobenzylamine was conducted to give the carbamoyl pyridone **3**. Insertion of a methoxy unit replacing the bromine was followed by Mitsunobu reaction with benzyl alcohol to give the intermediate **5**. Oxidation of the pyridine nitrogen with *m*-CPBA followed by thermal rearrangement of the *N*-oxide in acetic anhydride gave the corresponding hydroxymethyl derivative **7**. This material was oxidized by sulfur trioxide pyridine to give the corresponding aldehyde **8**. Concomitant oxidation-esterification using iodine in methanol provided the key intermediate **9**. Stepwise deprotection of the *O*-benzyl group by TMSI prepared in situ from TMSCl and NaI followed by removal of the methyl ether with aluminum trichloride concluded preparation of compound **11**. Alkaline hydrolysis of **11** led to the corresponding carboxylic acid **12**. Alternatively, treatment of the ester with an amine under microwave irradiation provided the corresponding amides (**13,14**). After alkaline hydrolysis of the intermediate **9**, coupling of the resulting acid with an amine using 1-ethyl-3-(3-dimethylaminopropyl)carbodiimide hydrochloride served to give the corresponding amides (**16–18**). Removal of the

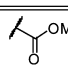
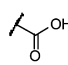
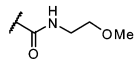
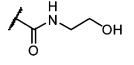
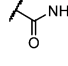
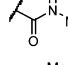
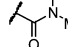
methyl group with pyridine–HCl at elevated temperature concluded preparation of compounds **19–21**.

## 4. RESULTS AND DISCUSSION

### 4.1. Efficacies in Enzymatic and Antiviral Assays.

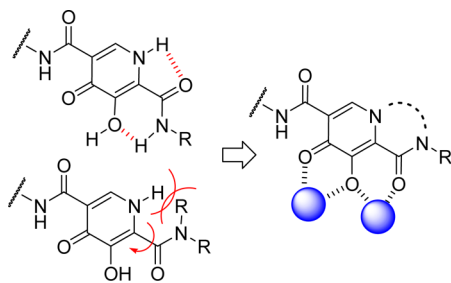
Inhibitory activities of carbamoyl pyridone inhibitors are summarized in Table 1. Compound **11**, which has an ester group as a metal coordinating unit, shows promising potencies in both enzyme and antiviral assays. The cell cytotoxicity selectivity index was large enough to establish a clear antiviral effect to justify progression to further evaluations. The corresponding carboxylic acid **12** had comparable potency to compound **11** in the enzymatic assay, however, results in a drastic loss of antiviral efficacy in the whole cell system. Low cellular penetration due to poor permeability of compound **12** is the most plausible explanation of the behavior. Modification of the C2 acid/ester group to an amide was an attractive approach to address the potential issue of chemical or metabolic stabilities of the ester unit and low permeability of the carboxylic acid. However, all amide derivatives in Table 1, including primary, secondary, and tertiary amides, showed potencies remarkably reduced in both enzymatic and antiviral

Table 1. Results in Enzyme and Cellular Assay<sup>a</sup>


Cmpd.	Structure	MWPA-Mg <sup>b</sup> IC <sub>50</sub> (nM)	MT-4/MTT <sup>c</sup> wild type IC <sub>50</sub> (nM)	MT-4/MTT <sup>d</sup> CC <sub>50</sub> (nM)
11		18±5.3	10 ± 2.9	19000 ± 850
12		10 <sup>e</sup>	1400 ± 400	>200000
13		130±42	110 ± 42	16000 ± 1400
14		300±100	5500 ± 3200	>200000
19		380±74	5500 ± 2400	40000 ± 3800
20		1300±860	120 ± 31	8500 ± 2000
21		540±210	1600 ± 510	5100 ± 460

<sup>a</sup>Data represent the mean ± sd from independent three experiments. <sup>b</sup>Strand transfer inhibitory activities. MWPA-Mg: microtiter plate integration assay with preincubation and wash using Mg<sup>2+</sup> as cofactors. <sup>c</sup>Anti-HIV activities using MT-4 cells. <sup>d</sup>Cytotoxicity using MT-4 cells. <sup>e</sup>The mean value from independent two experiments.

assays. The losses are not dependent on substituents on the amide unit but seem to be a result of the amide unit itself. A planar chelating core unit is required to effectively coordinate the active site metals,<sup>3,14</sup> however, as shown in Figure 6,



**Figure 6.** (left) Plausible explanation of insufficient inhibitory activities in amide modification. (right) The dotted line represents a potential next approach to address the amide scaffolds issue.

undesired intramolecular hydrogen bonding or steric hindrance is potentially the reason for diminished activity in some of our amide analogues. Tethering the amide back to the core scaffold is an attractive idea to address this issue and will be the subject of later publications.

#### 4.2. Antiviral Efficacy against Resistant Mutants and PK Profile of Compound 11.

Compound 11 showed promising antiviral efficacy in a wild type HIV-1 strain as shown in Table 1. Even in the presence of human serum albumin (HSA), a potency reduction of only 12-fold resulting gave a protein adjusted IC<sub>50</sub> (<sup>MT4</sup>PAIC<sub>50</sub>) of 120 nM (Table 2). On the contrary, the compound showed losses of efficacy against some of resistant mutants (200-fold change against Q148K, 21-fold against N155H, and 1.5-fold against Y143R), which represent or model clinically relevant RAL resistant variants. In particular, the Y143 data is consistent with a lack of dependence on interaction with the tyrosine 143 aromatic group as is the case for RAL but not for EVG.<sup>13</sup> While the resistance profile of 11 are still less than sufficient against the N155 and Q148 mutants to justify further progression, we have demonstrated a comparable or slightly improved profile when compared to RAL or EVG, with a very simple scaffold amendable to substantial further modification.<sup>16</sup> Animal PK studies were conducted for compound 11 with 1 mg/kg intravenous (iv) dosing and 5 mg/kg oral (po) dosing using fed conditions. Plasma concentrations were collected up to 24 h post dose. In rats, the compound has a total clearance (CL<sub>T</sub>) of 1.2 mL/min/kg and terminal half-life (*T*<sub>1/2</sub>) of 4.7 h from an iv dose. In the po studies, AUC<sub>0→∞</sub> of 41200 ng·h/mL, *T*<sub>1/2</sub> of 4.2

**Table 2. Fold Change in Antiviral Potency against Integrase Mutants for RAL, EVG, and Compound 11<sup>a</sup>**

compd	MT4/MTT wild type IC <sub>50</sub> (nM)	Q148K (FC)	N155H (FC)	Y143R (FC)	potency shift	<sup>MT4</sup> PAIC <sub>50</sub> (nM)
RAL	6.2 ± 2.2	83 ± 6.6 <sup>b</sup>	8.4 ± 1.8 <sup>b</sup>	16 ± 3.9 <sup>b</sup>	4.7 <sup>b</sup>	29
EVG	1.3 ± 0.35	>1700 <sup>b</sup>	25 ± 7.8 <sup>b</sup>	1.8 ± 0.16 <sup>b</sup>	22 <sup>b</sup>	29
11	10 ± 2.9	200 ± 25	21 ± 8.9	1.5 ± 0.59	12	120

<sup>a</sup>Data represent the mean ± sd. FC: fold change. <sup>b</sup>Data reported in ref 15.

Table 3. Animal PK Parameters of Compound 11<sup>a</sup>

	CLt (mL/min/kg)	T <sub>1/2</sub> (h)	Vdss (mL/kg)	%F	C <sub>24</sub> / <sup>MT4</sup> PAIC <sub>50</sub> <sup>50</sup>
rat (n = 3)	1.2 ± 0.41	4.7 ± 0.15	200 ± 38	53 ± 20	3.4 ± 2.5
dog (n = 3)	0.84 ± 0.17	3.8 ± 0.83	140 ± 30	46 ± 9.1	6.0 ± 4.6
cyno (n = 3)	2.4 ± 0.25	5.3 ± 1.00	300 ± 120	22 ± 6.4	1.6 ± 1.1

<sup>a</sup>Data represent the mean ± sd.

h, bioavailability of 53.4%, and most importantly 130 ng/mL of plasma concentration at 24 h postdosing (C<sub>24</sub>) were observed. The favorable exposure properties continued to manifest in beagle dogs and cynomolgus monkeys. Moderate molecular weight and good solubility properties suggested the carbamoyl pyridone model system contained good druglike properties (clogP = 0.63, ligand efficiency (pIC<sub>50</sub>/HAC) = 0.35). Additionally, no remarkable CYP inhibition nor metabolic concerns were identified during in vitro studies. The observation that the 24 h plasma concentration (C<sub>24</sub>) from a 5 mg/kg oral dose (130 ng/mL) robustly covered the <sup>MT4</sup>PAIC<sub>50</sub> of 38.4 ng/mL in every species gave us confidence that this newly designed scaffold was heading in the right direction to ultimately deliver once daily unboosted pharmacokinetics if we could fully optimize the antiviral profile against resistant variants.

## 5. CONCLUSIONS AND REMARKS

We succeeded in designing a carbamoyl pyridone scaffold as a novel inhibitor of HIV-1 integrase with high antiviral potency and a favorable protein binding effects. Although the compound 11 does not show the necessary potency against all the key resistant mutants, a promising PK profile suggesting once daily dosing was a significant attribute of the series and something we felt justified further optimization. Amide modifications were not successful, although it represents an attractive starting point for further study. Our advanced two-metal binding pharmacophore methodology has been quite useful in molecular design, producing an attractive new starting point for further optimization. Recent crystallography studies of a prototype foamy virus intasome with substrates and known integrase strand transfer inhibitors by Cherapanov et al.<sup>13</sup> have served as further validation of our basic pharmacophore model.

## 6. EXPERIMENTAL SECTION

**6.1. Chemistry.** Reactions were carried out under a nitrogen atmosphere with anhydrous solvents. Melting points were collected up to 300 °C with a Stanford Research Systems Optimet for every crystallized sample. Combustion analyses were performed with a Yanaco CORDER MT-6 and a DIONEX ICS-2000, and the analytical data confirmed purity of the tested samples to be ≥95%. <sup>1</sup>H NMR spectra were measured on a Varian MERCURY or Gemini 300 MHz spectrometer in a solution of either CDCl<sub>3</sub> or DMSO-*d*<sub>6</sub>, using tetramethylsilane as the internal standard. Chemical shifts are expressed as δ (ppm) values for protons relative to the internal standard.

**5-Bromo-4-hydroxy-6-methylnicotinic Acid (2).** To a solution of 4-hydroxy-6-methylnicotinic acid 1 (95.6 g, 0.625 mol) in acetic acid (950 mL) and water (190 mL), bromine (39 mL, 0.750 mol) was added over 15 min. After stirring at 60 °C for 5 h, the solvent was removed in vacuo. Residual solid was collected by filtration and washed with methanol (200 mL). The filtrate was evaporated in vacuo, and residual solid was collected by filtration and washed by methanol. The two portions were combined to give the product as colorless solid (142.2 g, 98% yield). <sup>1</sup>H NMR (DMSO-*d*<sub>6</sub>) δ 2.53 (s, 3H), 8.56 (s, 1H), 13.45 (brs, 1H), 14.80 (brs, 1H).

**5-Bromo-N-(4-fluorobenzyl)-4-hydroxy-6-methylnicotineamide (3).** To a solution of compound 2 (138 g, 0.596 mol), 1-ethyl-3-(3-dimethylaminopropyl)carbodiimide hydrochloride (148 g, 0.775 mol), and HOBt (100 g, 0.656 mol) in DMF (970 mL), 4-fluorobenzylamine (79 mL, 0.715 mol) was added. The reaction mixture was stirred at room temperature for 9 h, and water (2 L) was added. The residual solid was collected by filtration and washed with ether to give the product as colorless solid (156 g, 77% yield). <sup>1</sup>H NMR (DMSO-*d*<sub>6</sub>) δ 2.47 (s, 3H), 4.50 (d, J = 5.9 Hz, 2H), 7.12–7.20 (m, 2H), 7.32–7.39 (m, 2H), 8.38 (s, 1H), 10.50 (t, J = 5.9 Hz, 1H), 12.72 (brs 1H).

**N-(4-Fluorobenzyl)-4-hydroxy-5-methoxy-6-methylnicotineamide (4).** To a solution of compound 3 (75.2 g, 222 mmol) and copper(I) iodide (21.1 g, 111 mmol) in DMF (750 mL), a 28% NaOMe solution in methanol (216 mL, 888 mmol) was added. The reaction mixture was stirred at 105 °C for 100 min. After cooling, ice water (800 mL) was added, and undesired precipitate was filtrated off. Then 2 M aq HCl (443 mL) was added to the filtrate. Precipitate was collected by filtration to give the product as colorless solid (56.0 g, 87% yield). <sup>1</sup>H NMR (DMSO-*d*<sub>6</sub>) δ 2.26 (s, 3H), 3.74 (s, 3H), 4.49 (d, J = 6.0 Hz, 2H), 7.10–7.19 (m, 2H), 7.30–7.38 (m, 2H), 8.24 (s, 1H), 10.68 (t, J = 6.0 Hz, 1H), 12.21 (brs, 1H).

**4-Benzyloxy-N-(4-fluorobenzyl)-5-methoxy-6-methylnicotineamide (5).** To a solution of the compound 4 (100 g, 344 mmol), BnOH (46 mL, 447 mmol), and *n*-Bu<sub>3</sub>P (128 mL, 516 mmol) in THF (1.0 L), a 40% DIAD solution in toluene (280 mL, 516 mmol) was added over 30 min under ice-cooling. After stirring for 30 min under ice-cooling, the mixture was stirred under reflux condition for 2 h. After evaporation of the solvent in vacuo, toluene (100 mL) and *n*-hexane (2 L) were added to the residue, and precipitate was filtered off. After evaporation of the solvent in vacuo, Et<sub>2</sub>O (200 mL) and *n*-hexane (2 L) were added to the residue. Precipitation was again filtered off. After evaporation of the solvent, the residue was purified by silica gel column chromatography (*n*-hexane:ethyl acetate/1:3) to give the product as colorless solids (68.5 g, 52% yield). <sup>1</sup>H NMR (CDCl<sub>3</sub>) δ 2.58 (s, 3H), 3.86 (s, 3H), 4.40 (d, J = 5.7 Hz, 2H), 5.21 (s, 2H), 6.91–7.00 (m, 2H), 7.08–7.14 (m, 2H), 7.19–7.27 (m, 2H), 7.32–7.40 (m, 3H), 7.87 (brs, 1H), 8.97 (s, 1H).

**4-Benzyloxy-N-(4-fluorobenzyl)-5-methoxy-6-methyl-N-oxynicotineamide (6).** To a solution of the compound 5 (67.5 g, 177 mmol) in chloroform (350 mL), a 65% solution of *m*-CPBA (49.5 g, 186 mmol) in chloroform (350 mL) was added over 30 min under ice-cooling. After stirring for 45 min under ice-cooling, the reaction mixture was stirred further at room temperature for 75 min. To the reaction mixture, a saturated aq Na<sub>2</sub>CO<sub>3</sub> solution was added and extracted with chloroform. The organic layer was washed with a saturated aq Na<sub>2</sub>CO<sub>3</sub> solution and dried with anhydrous Na<sub>2</sub>SO<sub>4</sub>. The solvent was evaporated in vacuo, and residual crystals were collected by filtration and washed by Et<sub>2</sub>O (47.8 g). The filtrate was evaporated in vacuo, and residue was purified by silica gel column chromatography (toluene:acetone/1:1–1:3) to give 2.65 g of crystals. The two portions of crystals were combined to give the product (50.5 g, 72% yield); mp 138–139 °C. <sup>1</sup>H NMR (CDCl<sub>3</sub>) δ 2.55 (s, 3H), 3.90 (s, 3H), 4.40 (d, J = 5.7 Hz, 2H), 5.16 (s, 2H), 6.93–6.70 (s, 2H), 6.90–7.19 (m, 5H), 7.30–7.38 (m, 2H), 7.94 (brs, 1H), 8.81 (s, 1H). Anal. Calcd for C<sub>22</sub>H<sub>21</sub>FN<sub>3</sub>O<sub>4</sub>(H<sub>2</sub>O)<sub>0.1</sub>: C, 66.36; H, 5.37; F, 4.77; N, 7.03. Found: C, 66.27; H, 5.30; F, 4.55; N, 7.04.

**4-Benzyloxy-N-(fluorobenzyl)-6-hydroxymethyl-5-methoxynicotineamide (7).** A solution of the compound 6 (49.4 g, 125 mmol) in acetic anhydride (350 mL) was stirred at 80 °C for 30 min. Acetic anhydride was evaporated in vacuo. The residue was dissolved in methanol (500 mL), and a 28% solution of NaOMe in methanol (7.5 mL, 31.3 mmol) was added under ice-cooling. The mixture was stirred

at room temperature for 1 h. Amberlite IR-120B was added to the solution until the solution became neutral. After filtration of a residual precipitate, the filtrate was evaporated in vacuo. The residue was purified by silica gel column chromatography (*n*-hexane:ethyl acetate/1:1–1:3) to give the product as colorless crystals (25.4 g, 51% yield); mp 242–244 °C. <sup>1</sup>H NMR (CDCl<sub>3</sub>) δ 3.42 (brs, 1H), 3.89 (s, 3H), 4.41 (d, *J* = 5.7 Hz, 2H), 4.83 (s, 2H), 5.23 (s, 2H), 6.92–6.99 (m, 2H), 7.09–7.14 (m, 2H), 7.19–7.23 (m, 2H), 7.28–7.37 (m, 3H), 7.85 (brs, 1H), 9.03 (s, 1H). Anal. Calcd for C<sub>22</sub>H<sub>21</sub>FN<sub>2</sub>O<sub>4</sub>(H<sub>2</sub>O)<sub>0.3</sub>: C, 65.76; H, 5.42; F, 4.73; N, 6.97. Found: C, 65.89; H, 5.32; F, 4.59; N, 7.10.

**4-Benzoyloxy-N-(4-fluorobenzyl)-6-formyl-5-methoxynicotinea-mide (8).** To a solution of the compound 7 (25.0 g, 63.1 mmol), DMSO (44.8 mL, 631 mmol), and Et<sub>3</sub>N (44.3 mL, 378 mmol) in chloroform (250 mL), SO<sub>3</sub>–pyridine complex (50.2 g, 315 mmol) was added under ice-cooling. The reaction mixture was stirred at room temperature for 20 min. Water was added to the reaction mixture, and chloroform was evaporated in vacuo. The residual aqueous solution was extracted with ethyl acetate, and the extract was washed with water. The organic layer was dried with anhydrous Na<sub>2</sub>SO<sub>4</sub>. The solvent was evaporated in vacuo, and residual crystals (17.7 g) were collected by filtration and washed by Et<sub>2</sub>O. The filtrate was evaporated in vacuo, and precipitate was purified by silica gel column chromatography to give another portion of crystals (3.16 g). Two portions were combined to give the product as colorless crystals (20.9 g, 84% yield); mp 99–100 °C. <sup>1</sup>H NMR (CDCl<sub>3</sub>) δ 4.02 (s, 3H), 4.41 (d, *J* = 5.7 Hz, 2H), 5.30 (s, 2H), 6.93–6.70 (m, 2H), 7.09–7.15 (m, 2H), 7.20–7.27 (m, 2H), 7.31–7.40 (m, 3H), 7.83 (brs, 1H), 9.20 (s, 1H), 10.26 (s, 1H). Anal. Calcd for C<sub>22</sub>H<sub>19</sub>FN<sub>2</sub>O<sub>4</sub>: C, 67.00; H, 4.86; F, 4.82; N, 7.10. Found: C, 66.85; H, 4.86; F, 4.63; N, 7.06.

**Methyl 4-Benzoyloxy-5-(4-fluorobenzylcarbamoyl)-3-methoxy-pyridine-2-carboxylate (9).** To a solution of the compound 8 (300 mg, 0.761 mmol) in methanol (1 mL), a solution of KOH (111 mg, 1.99 mmol) in methanol (1 mL) was added under ice-cooling, and then a solution of iodine (251 mg, 1.00 mmol) in methanol (4 mL) was added. The mixture was stirred under ice-cooling for 1 h. A 5% (w/v) solution of aq NaHSO<sub>3</sub> and water were added to the reaction mixture. Precipitate was collected by filtration to give the product as colorless crystals (275 mg, 85% yield); mp 75–78 °C. <sup>1</sup>H NMR (CDCl<sub>3</sub>) δ 3.99 (s, 3H), 4.02 (s, 3H), 7.40 (d, *J* = 5.7 Hz, 2H), 5.26 (s, 2H), 6.92–6.99 (m, 2H), 7.10–7.15 (m, 2H), 7.19–7.23 (m, 2H), 7.25–7.39 (m, 3H), 7.81 (brs, 1H), 9.09 (s, 1H). Anal. Calcd for C<sub>23</sub>H<sub>21</sub>FN<sub>2</sub>O<sub>5</sub>(H<sub>2</sub>O)<sub>0.4</sub>: C, 64.00; H, 5.09; F, 4.40; N, 6.49. Found: C, 63.95; H, 4.89; F, 4.37; N, 6.69.

**Methyl 5-(4-Fluorobenzylcarbamoyl)-3-methoxy-4-oxo-1,4-dihydropyridine-2-carboxylate (10).** To a suspension of sodium iodide (5.51 g, 36.8 mmol) in acetonitrile (50 mL), chlorotrimethylsilane (4.66 mL, 36.8 mmol) was added. The reaction mixture was stirred at room temperature for 10 min. To this solution the compound 9 (2.60 g, 6.13 mmol) was added under ice-cooling, and the mixture was stirred at the same temperature for 20 min. To the reaction solution a 5% (w/v) solution of aq NaHSO<sub>3</sub> was added and then extracted with ethyl acetate. The extract was washed with a saturated aq Na<sub>2</sub>CO<sub>3</sub> and a saturated aq NaCl and dried with anhydrous Na<sub>2</sub>SO<sub>4</sub>. The solvent was evaporated in vacuo, and the precipitate was recrystallized (acetone–diisopropyl ether) to give the product as colorless crystals (1.73 g, 84% yield); mp 183–184 °C. <sup>1</sup>H NMR (CDCl<sub>3</sub>) δ 4.04 (s, 6H), 4.60 (d, *J* = 6.0 Hz, 2H), 6.96–7.03 (m, 2H), 7.29–7.35 (m, 2H), 8.63 (s, 1H), 9.68 (s, 1H), 10.34 (brs, 1H). Anal. Calcd for C<sub>16</sub>H<sub>15</sub>FN<sub>2</sub>O<sub>5</sub>: C, 57.48; H, 4.52; F, 5.68; N, 8.38. Found: C, 57.34; H, 4.50; F, 5.46; N, 8.39.

**Methyl 5-(4-Fluorobenzylcarbamoyl)-3-hydroxy-4-oxo-1,4-dihydropyridine-2-carboxylate (11).** To a solution of the compound 10 (1.73 g, 5.17 mmol) in dichloromethane (150 mL) was added aluminum chloride (6.97 g, 51.7 mmol), and the mixture was stirred at room temperature for 2 h. The reaction mixture was poured into 2 M aq HCl containing an ice, followed by extraction with ethyl acetate. The extract was washed with 2 M aq HCl and water and then dried with anhydrous Na<sub>2</sub>SO<sub>4</sub>. The solvent was removed in vacuo, and the precipitate was recrystallized (THF–methanol) to give the product as

colorless crystals (919 mg, 56% yield); mp 242–244 °C. <sup>1</sup>H NMR (DMSO-*d*<sub>6</sub>) δ 3.91 (s, 3H), 4.52 (d, *J* = 5.8 Hz, 2H), 7.12–7.19 (m, 2H), 7.34–7.40 (m, 2H), 8.19–8.22 (m, 1H), 10.12 (brs, 1H), 10.20 (d, *J* = 5.8 Hz, 1H), 12.43 (brs, 1H). Anal. Calcd for C<sub>15</sub>H<sub>13</sub>FN<sub>2</sub>O<sub>5</sub>: C, 56.25; H, 4.09; F, 5.93; N, 8.75. Found: C, 56.00; H, 4.03; F, 5.58; N, 8.69.

**5-(4-Fluorobenzylcarbamoyl)-3-hydroxy-4-oxo-1,4-dihydropyridine-2-carboxylic Acid (12).** To a solution of the compound 11 (100 mg, 0.31 mmol) in methanol (3 mL), 1 M aq LiOH (1 mL) was added at room temperature. The reaction mixture was stirred for 2 h at 60 °C. After being cooled down by ice–water, 2 M aq HCl (1 mL) was added. Precipitated crystals were collected and washed with water to give the product as colorless crystals (91 mg, 96% yield); mp 221–222 °C. <sup>1</sup>H NMR (DMSO-*d*<sub>6</sub>) δ 4.51 (d, *J* = 5.7 Hz, 2H), 7.12–7.19 (m, 2H), 7.33–7.39 (m, 2H), 8.17 (s, 1H). Anal. Calcd for C<sub>14</sub>H<sub>11</sub>FN<sub>2</sub>O<sub>5</sub>(H<sub>2</sub>O)<sub>1.0</sub>: C, 51.86; H, 4.04; F, 5.86; N, 8.64. Found: C, 51.78; H, 3.98; F, 5.78; N, 8.64.

**3-Hydroxy-4-oxo-1,4-dihydro-pyridine-2,5-dicarboxylic Acid 5-(4-Fluorobenzylamide) 2-(2-methoxyethyl)amide (13).** To a solution of the compound 11 (96 mg, 0.3 mmol) in methanol (3 mL), 2-methoxyethanamine (113 mg, 1.5 mmol) was added. The reaction was performed with a microwave reaction apparatus at 140 °C for 15 min. After being cooled to room temperature, 2 M aq HCl (3 mL) was added. Precipitate was collected by filtration and washed by water to give the product as colorless crystals (101 mg, 93% yield); mp 295–299 °C. <sup>1</sup>H NMR (DMSO-*d*<sub>6</sub>) δ 3.28 (s, 3H), 3.39–3.62 (m, 4H), 4.52 (d, *J* = 5.9 Hz, 2H), 7.14–7.20 (m, 2H), 7.35–7.39 (m, 2H), 8.24 (d, *J* = 7.2 Hz, 1H), 8.46 (t, *J* = 5.2 Hz, 1H), 10.32 (t, *J* = 5.8 Hz, 1H), 12.23 (d, *J* = 5.8 Hz, 1H). Anal. Calcd for C<sub>17</sub>H<sub>18</sub>FN<sub>3</sub>O<sub>5</sub>: C, 56.20; H, 4.99; F, 5.23; N, 11.56. Found: C, 55.86; H, 4.87; F, 5.10; N, 11.39.

**3-Hydroxy-4-oxo-1,4-dihydropyridine-2,5-dicarboxylic Acid 5-(4-Fluorobenzylamide) 2-[(2-hydroxyethyl)amide] (14).** This compound was prepared in a similar manner to that described for 13 (colorless crystals, 96 mg, 89% yield); mp 285–287 °C. <sup>1</sup>H NMR (DMSO-*d*<sub>6</sub>) δ 3.44–3.61 (m, 4H), 4.53 (d, *J* = 6.0 Hz, 2H), 4.91 (s, 1H), 7.13–7.21 (m, 2H), 7.35–7.40 (m, 2H), 8.24 (s, 1H), 8.53 (s, 1H), 10.34 (t, *J* = 5.7 Hz, 1H), 12.23 (brs, 1H). Anal. Calcd for C<sub>16</sub>H<sub>16</sub>FN<sub>3</sub>O<sub>5</sub>: C, 55.01; H, 4.62; F, 5.44; N, 12.03. Found: C, 54.71; H, 4.58; F, 5.28; N, 11.96.

**4-Benzoyloxy-5-(4-fluorobenzylcarbamoyl)-3-methoxypyridine-2-carboxylic Acid (15).** To a solution of the compound 9 (900 mg, 2.12 mmol) in methanol (8 mL), a 2 M aq NaOH (4 mL) was added. The reaction solution was stirred at room temperature for 2 h, and 2 M aq HCl (3 mL) was added. Precipitate was collected by filtration to give the product as colorless crystals (474 mg, 54% yield); mp 138–139 °C. <sup>1</sup>H NMR (CDCl<sub>3</sub>) δ 4.05 (s, 3H), 4.40 (d, *J* = 5.6 Hz, 2H), 5.36 (s, 2H), 6.94–7.01 (m, 2H), 7.08–7.12 (m, 2H), 7.21–7.24 (m, 2H), 7.29–7.41 (m, 3H), 7.87 (brs, 1H), 9.03 (s, 1H). Anal. Calcd for C<sub>22</sub>H<sub>19</sub>FN<sub>2</sub>O<sub>5</sub>: C, 64.39; H, 4.67; F, 4.63; N, 6.83. Found: C, 64.35; H, 4.62; F, 4.41; N, 6.87.

**3-Hydroxy-4-oxo-1,4-dihydropyridine-2,5-dicarboxylic Acid 2-Amide 5-(4-fluorobenzyl)amide (19).** The compound 15 (155 mg, 0.378 mmol), 2-ethyl-3-(3-dimethylaminopropyl)carbodiimide hydrochloride (87 mg, 0.453 mmol), and 1-hydroxybenzotriazole (61 mg, 0.453 mmol) were dissolved in DMF (2 mL), and the solution was stirred at room temperature for 30 min. Thereafter, ammonium chloride (40 mg, 0.756 mmol) and diisopropylethylamine (198 μL, 1.13 mmol) were added. The reaction solution was stirred at room temperature for 1 h. Water was added to the solution, and precipitate was collected by filtration and washed with Et<sub>2</sub>O to give crude product 16 of 127 mg. Directly to 16 pyridine–HCl (1.27 g) was added and then heated at 180 °C for 5 min. After cooling the reaction mixture to room temperature, water was added. Precipitate was collected by filtration and washed with Et<sub>2</sub>O to give the product as skin-colored crystals (88 mg, 76% yield for two steps); mp higher than 300 °C. <sup>1</sup>H NMR (DMSO-*d*<sub>6</sub>) δ 4.53 (d, *J* = 5.6 Hz, 2H), 7.14–7.20 (m, 2H), 7.35–7.40 (m, 2H), 7.79 (s, 1H), 8.24 (d, *J* = 7.0 Hz, 1H), 8.33 (s, 1H), 10.33 (t, *J* = 5.6 Hz, 1H), 12.23 (d, *J* = 7.0 Hz, 1H). Anal. Calcd for C<sub>14</sub>H<sub>12</sub>FN<sub>3</sub>O<sub>4</sub>(H<sub>2</sub>O)<sub>0.2</sub>: C, 54.44; H, 4.05; F, 6.15; N, 13.60. Found: C, 54.82; H, 3.96; F, 5.75; N, 13.53

**3-Hydroxy-4-oxo-1,4-dihydropyridine-2,5-dicarboxylic Acid 5-(4-Fluorobenzyl)amide 2-methylamide (20).** This compound was prepared in a similar manner to that described for **19** (colorless crystals 89 mg, 92% yield for two steps); mp higher than 300 °C. <sup>1</sup>H NMR (DMSO-*d*<sub>6</sub>) δ 2.91 (d, *J* = 4.7 Hz, 3H), 4.53 (d, *J* = 5.8 Hz, 2H), 7.14–7.20 (m, 2H), 7.35–7.40 (m, 2H), 8.23–8.25 (m, 1H), 8.35 (d, *J* = 5.0 Hz, 1H), 10.35 (t, *J* = 5.8 Hz, 1H), 12.23 (d, *J* = 6.3 Hz, 1H). Anal. Calcd for C<sub>15</sub>H<sub>14</sub>FN<sub>3</sub>O<sub>4</sub>: C, 56.43; H, 4.42; F, 5.95; N, 13.16. Found: C, 56.18; H, 4.36; F, 5.63; N, 12.96.

**3-Hydroxy-4-oxo-1,4-dihydropyridine-2,5-dicarboxylic Acid 2-Di-methylamide 5-(4-Fluorobenzyl)amide (21).** This compound was prepared in a similar manner to that described for **19** (colorless crystals 80 mg, 64% yield); mp 269–270 °C. <sup>1</sup>H NMR (DMSO-*d*<sub>6</sub>) δ 2.92 (s, 3H), 3.00 (s, 3H), 4.53 (d, *J* = 5.8 Hz, 2H), 7.13–7.19 (m, 2H), 7.34–7.39 (m, 2H), 8.19–8.21 (m, 1H), 9.63 (brs, 1H), 10.44 (t, *J* = 5.8 Hz, 1H), 12.60 (brs, 1H). Anal. Calcd for C<sub>16</sub>H<sub>16</sub>FN<sub>3</sub>O<sub>4</sub>: C, 57.65; H, 4.84; F, 5.70; N, 12.61. Found: C, 57.44; H, 4.79; F, 5.40; N, 12.41.

**6.2. Biological Assay. Cells and Viruses.** HeLa–CD4 cells carrying reporter β-galactosidase gene driven by HIV-1 LTR were established by transfection of HeLa cells with CD4 and β-galactosidase expression vector.<sup>17</sup> Molt-4 cells persistently infected with HIV-1 strain IIIB<sup>18</sup> and human T cell line MT-4 cells were obtained from the Institute for Virus Research, Kyoto University. 293T cells and HeLa–CD4 cells were maintained in Dulbecco's Modified Eagle Medium (DMEM) supplemented with 10% fetal bovine serum (FBS) and 100 μg/mL kanamycin sulfate. Molt-4 cells and MT-4 cells were maintained in RPMI 1640 medium supplemented with 10% FBS and 100 μg/mL kanamycin sulfate.

**Enzyme Assay.** The assay method used included preformation of IN-substrate DNA complex on a microtiter plate and washing out of the unbound IN protein (MWPA = microtiter plate integration assay with preincubation and wash). In brief, after formation of the IN–DNA complex and washing out of unbound IN, a test compound was added to integration reaction buffer (10 mM dithiothreitol, 5% glycerol, 100 μg/mL bovine serum albumin, 30 mM MOPS, pH 7.2), and the plate was incubated at 30 °C for 30 min in order to let the compound bind to the IN–DNA complex. Then, digoxigenin (Dig) labeled target DNA was added to the reaction mixture to initiate the strand transfer reaction. The amount of strand transfer products was estimated by a standard enzyme linked immune assay with anti-Dig antibody. We used magnesium (Mg<sup>2+</sup>, 15 mM) as a cofactor through all steps, and we name it MWPA with Mg assay (MWPA-Mg).

**Antiviral Assay.** MT-4 cells of 2.5 × 10<sup>4</sup> cells/well were aliquoted to 96-well plates in the presence of varying concentrations of compounds. After incubation for 1 h, HIV-1 strain IIIB at a viral multiplicity of infection of 0.001 or a 50% tissue culture infectious dose of 4 to 10 was added to plate. After incubation for 4 days, the antiviral activity was evaluated as a cell viability measured by absorbance at 560 and 690 nm using the yellow tetrazolium MTT reagent [(3-(4,5-dimethylthiazol-2-yl)-2,5-diphenyltetrazolium bromide)].

**Effect of Human Serum and Serum Proteins.** The potency shift of the antiviral activity of each compound with the presence of human serum albumin (HSA; 20 mg/mL) was evaluated in the MT-4 assay systems. The protein-adjusted half-maximal inhibitory concentration (<sup>MT4</sup>PAIC<sub>50</sub>) was estimated by multiplying the IC<sub>50</sub> value in routine MT4 assay by the fold-shift value.

**Cell Cytotoxicity Assays.** In vitro growth inhibition (cytotoxicity) studies were conducted in MT-4 cells. MT-4 cells of 2.5 × 10<sup>4</sup> cells/well were aliquoted to 96-well plates in the presence of varying concentrations of compounds. After incubation for 4 days, cell bioavailability was measured by absorbance at 560 and 690 nm using the yellow tetrazolium MTT reagent to evaluate the ability of a compound to inhibit cell growth as an indicator of a compound's potential for cytotoxicity.

**Resistance Profiling.** Recombinant HIV-1 molecular clones were constructed by introducing mutations into the integrase-coding region of pNL432 as described previously.<sup>14</sup> Plasmids were subsequently transfected into 293T cells to generate infectious virus. Supernatants were harvested after 2 days of culture and stored as cell-free culture

supernatants at –80 °C. Compounds were evaluated against molecular clones with mutations in the integrase-coding regions. INI-resistant mutants were analyzed by the reporter assay based on HeLa–CD4 cells.

**6.3. PK Studies in Rats, Dogs, and Monkeys.** For po administration studies in rats, dogs, and monkeys, compound was dissolved in DMSO/Solutol/50 mM *N*-methylglucamine in 5% mannitol (15/15/70, v/w/v). Compound was dissolved in DMA/PEG/saline (1:4:5, by vol) for rat iv administration and was dissolved in 50 mM *N*-methylglucamine in 3% mannitol for dog and monkey studies.

In rats PK study, rats were implanted with an indwelling cannula (silicone rubber/polyethylene) in the right jugular vein for blood sampling under anesthesia with ether on 3 days before the administration. Rats, dogs, and monkeys were administered compound at doses of 1 mg/kg for iv and 5 mg/kg for po administration.

Blood samples (approximately 0.3 mL) were collected at designated periods after administration and were immediately centrifuged at 16000g for 3 min to obtain plasma. The plasma samples were kept at –20 °C until analysis. The PK parameters of compound after iv and po administration were estimated using WinNonlin (Pharsight, Mountain View, CA, USA) by noncompartment analysis. AUC was calculated by the linear trapezoidal rule.

## AUTHOR INFORMATION

### Corresponding Author

\*Phone: +81-6-6331-6349. Fax: +81-6-6332-6385. E-mail: takashi.kawasuji@shionogi.co.jp.

### Notes

The authors declare no competing financial interest.

## ACKNOWLEDGMENTS

We thank all scientists in the Shionogi–GlaxoSmithKline research collaboration team for great discussions, in particular Shuji Iwashita and Eri Kanaoka for PK evaluations and Akemi Kagitani-Suyama, Shigeru Miki, and Shinobu Miki-Kawauchi for antiviral evaluations.

## ABBREVIATIONS USED

CYP3A, cytochrome P450, family 3, subfamily A; HOBt, 1-hydroxybenzotriazole; rt, room temperature; NaOMe, sodium methoxide; BnOH, benzyl alcohol; DIAD, diisopropyl azodicarboxylate; TMSI, trimethylsilyl iodide; TMSCl, trimethylsilyl chloride; NaI, sodium iodide; HAC, heavy atom count; *n*-Bu<sub>3</sub>P, *tri*-butylphosphine; Ac<sub>2</sub>O, acetic anhydride; AlCl<sub>3</sub>, trichloro aluminum; KOH, potassium hydroxide; NaOH, sodium hydroxide; LiOH, lithium hydroxide; Et<sub>3</sub>N, triethylamine; CDCl<sub>3</sub>, deuterated chloroform; DMSO-*d*<sub>6</sub>, deuterated DMSO; HCl, hydrogen chloride; Na<sub>2</sub>CO<sub>3</sub>, sodium carbonate; Na<sub>2</sub>SO<sub>4</sub>, sodium sulfate; Et<sub>2</sub>O, diethyl ether; NaHSO<sub>3</sub>, sodium hydrogen sulfite; MOPS, 3-morpholinopropanesulfonic acid

## REFERENCES

- (1) (a) De Clercq, E. New Anti-HIV Agents and Targets. *Med. Res. Rev.* **2002**, *22* (6), 531–565. (b) De Clercq, E. Highlights in the Development of New Antiviral Agents. *Mini-Rev. Med. Chem.* **2002**, *2*, 163–175. (c) Pani, A.; Loi, A. G.; Mura, M.; Marceddu, T.; La Colla, P.; Marongiu, M. E. Targeting HIV: Old and New Players. *Curr. Drug Targets–Infect. Disord.* **2002**, *2*, 17–32.
- (2) (a) Chiu, T. K.; Davies, D. R. Structure and Function of HIV-1 Integrase. *Curr. Top. Med. Chem.* **2004**, *4*, 965–977. (b) Craigie, R. HIV Integrase, a Brief Overview from Chemistry to Therapeutics. *J. Biol. Chem.* **2001**, *276*, 23213–23216. (c) Grobler, J. A.; Stillmock, K.; Hu, B.; Witmer, M.; Felock, P.; Espeseth, A. S.; Wolfe, A.; Egbertson, M.; Bourgeois, M.; Melamed, J.; Wai, J. S.; Young, S.; Vacca, J.; Hazuda, D. J. Diketo Acid Inhibitor Mechanism and HIV-1 Integrase:



Implications for Metal Binding in the Active Site of Phosphotransferase Enzymes. *Proc. Natl. Acad. Sci. U. S. A.* **2002**, *99*, 6661–6666.

(3) (a) Kawasuji, T.; Fuji, M.; Yoshinaga, T.; Sato, A.; Fujiwara, T.; Kiyama, R. A Platform for Designing HIV Integrase Inhibitors. Part 2: A Two-Metal Binding Model as a Potential Mechanism of HIV Integrase Inhibitors. *Bioorg. Med. Chem.* **2006**, *14*, 8420–8429. (b) Kawasuji, T.; Yoshinaga, T.; Sato, A.; Yodo, M.; Fujiwara, T.; Kiyama, R. A Platform for Designing HIV Integrase Inhibitors. Part 1: 2-Hydroxy-3-heteroaryl Acrylic Acid Derivatives as Novel HIV Integrase Inhibitor and Modeling of Hydrophilic and Hydrophobic Pharmacophores. *Bioorg. Med. Chem.* **2006**, *14*, 8430–8445.

(4) (a) Pendri, A.; Meanwell, N. A.; Peese, K. M.; Walker, M. A. New First and Second Generation Inhibitors of Human Immunodeficiency Virus-1 Integrase. *Expert Opin. Ther. Pat.* **2011**, *21*, 1173–1189. (b) Johns, B. A.; Svoltlo, A. C. Advances in Two-Metal Chelation Inhibitors of HIV Integrase. *Expert Opin. Ther. Pat.* **2008**, *18*, 1225–1237.

(5) (a) Rowley, M. The Discovery of Raltegravir, an Integrase Inhibitor for the Treatment of HIV Infection. *Prog. Med. Chem.* **2008**, *46*, 1–28. (b) Summa, V.; Petrocchi, A.; Bonelli, F.; Crescenzi, B.; Donghi, M.; Ferrara, M.; Fiore, F.; Gardelli, C.; Gonzalez Paz, O.; Hazuda, D. J.; Jones, P.; Kinzel, O.; Laufer, R.; Monteagudo, E.; Muraglia, E.; Nizi, E.; Orvieto, F.; Pace, P.; Pescatore, G.; Scarpelli, R.; Stillmock, K.; Witmer, M. V.; Rowley, M. Discovery of Raltegravir, a Potent, Selective Orally Bioavailable HIV-Integrase Inhibitor for the Treatment of HIV-AIDS Infection. *J. Med. Chem.* **2008**, *51*, 5843–5855.

(6) (a) Thompson, M. A.; Aberg, J. A.; Cahn, P.; Montaner, J. S.; Rizzardini, G.; Telenti, A.; Gatell, J. M.; Günthard, H. F.; Hammer, S. M.; Hirsch, M. S.; Jacobsen, D. M.; Reiss, P.; Richman, D. D.; Volberding, P. A.; Yeni, P.; Schooley, R. T. Antiretroviral Treatment of Adult HIV Infection: 2010 Recommendations of the International AIDS Society-USA panel. *JAMA, J. Am. Med. Assoc.* **2010**, *304*, 321–333. (b) Zolopa, A. The Evolution of HIV Treatment Guidelines: Current State-of-the-Art of ART. *Antiviral Res.* **2010**, *85*, 241–244.

(7) (a) Wainberg, M. A.; Zaharatos, G. J.; Brenner, B. G. Development of Antiretroviral Drug Resistance. *N. Engl. J. Med.* **2011**, *365*, 637–646. (b) Marcelin, A. G.; Ceccherini Silberstein, F.; Perno, C. F.; Calvez, V. Resistance to Novel Drug Classes. *Curr. Opin. HIV AIDS* **2009**, *4*, 531–537. (c) Métifiot, M.; Maddali, K.; Naumova, A.; Zhang, X.; Marchand, C.; Pommier, Y. Biochemical and Pharmacological Analyses of HIV-1 Integrase Flexible Loop Mutants Resistant to Raltegravir. *Biochemistry* **2010**, *49*, 3715–3722.

(8) (a) Shimura, K.; Kodama, E.; Sakagami, Y.; Matsuzaki, Y.; Watanabe, W.; Yamataka, K.; Watanabe, Y.; Ohata, Y.; Doi, S.; Sato, M.; Kano, M.; Ikeda, S.; Matsuoka, M. Broad Antiretroviral Activity and Resistance Profile of the Novel Human Immunodeficiency Virus Integrase Inhibitor Elvitegravir (JTK-303/GS-9137). *J. Virol.* **2008**, *82*, 764–774. (b) Sato, M.; Kawakami, H.; Motomura, T.; Aramaki, H.; Matsuda, T.; Yamashita, M.; Ito, Y.; Matsuzaki, Y.; Yamataka, K.; Ikeda, S.; Shinkai, H. Quinolone Carboxylic Acids as a Novel Monoketo Acid Class of Human Immunodeficiency Virus Type 1 Integrase Inhibitors. *J. Med. Chem.* **2009**, *52*, 4869–4882.

(9) (a) Elion, R.; Gathe, J.; Rashbaum, B.; Shalit, P.; Hawkins, T.; Liu, H.; Zhong, L.; Warren, D.; Kearney, B.; Chuck, S. The Single-Tablet Regimen Elvitegravir/Cobicistat/Emtricitabine/Tenofovir Disoproxil Fumarate (EVG/COBI/FTC/TDF; “QUAD”) Maintains a High Rate of Virologic Suppression, and Cobicistat (COBI) is an Effective Pharmacoenhancer through 48 Weeks. 50th Interscience Conference on Antimicrobial Agents and Chemotherapy, Boston, MA, 12–15 September 2010. (b) Cohen, C.; Shamblaw, D.; Ruane, P.; Elion, R.; DeJesus, E.; Liu, H.; Zhong, L.; Warren, D.; Kearney, B.; Chuck, S. Single-Tablet, Fixed-Dose Regimen of Elvitegravir/Emtricitabine/Tenofovir Disoproxil Fumarate/GS-9350 Achieves a High Rate of Virologic Suppression and GS-9350 is an Effective Booster. 17th Conference on Retroviruses and Opportunistic Infections, San Francisco, CA, 16–19 February 2010.

(10) (a) Goethals, O.; Clayton, R.; Van Ginderen, M.; Vereyken, I.; Wagemans, E.; Geluykens, P.; Dockx, K.; Strijbos, R.; Smits, V.; Vos,

A.; Meersseman, G.; Jochmans, D.; Vermeire, K.; Schols, D.; Hallenberger, S.; Hertogs, K. Resistance Mutations in Human Immunodeficiency Virus Type 1 Integrase Selected with Elvitegravir Confer Reduced Susceptibility to a Wide Range of Integrase Inhibitors. *J. Virol.* **2008**, *82*, 10366–10374. (b) Shimura, K.; Kodama, E.; Sakagami, Y.; Matsuzaki, Y.; Watanabe, W.; Yamataka, K.; Watanabe, Y.; Ohata, Y.; Doi, S.; Sato, M.; Kano, M.; Ikeda, S.; Matuoka, M. Broad Antiretroviral Activity and Resistance Profile of the Novel Human Immunodeficiency Virus Integrase Inhibitor Elvitegravir (JTK-303/GS-9137). *J. Virol.* **2008**, *82*, 764–774. (c) Hombrouch, A.; Voet, A.; Van Remoortel, B.; Desadeleer, C.; De Maeyer, M.; Debyser, Z.; Witvrouw, M. Mutations in Human Immunodeficiency Virus Type 1 Integrase Confer Resistance to the Naphthyridine L-870,810 and Cross-Resistance to the Clinical Trial Drug GS-9137. *Antimicrob. Agents Chemother.* **2008**, *52*, 2069–2078. (d) Marinello, J.; Marchand, C.; Mott, B. T.; Bain, A.; Thomas, C. J.; Pommier, Y. Comparison of Raltegravir and Elvitegravir on HIV-1 Integrase Catalytic Reactions and on a Series of Drug-Resistant Integrase Mutants. *Biochemistry* **2008**, *47*, 9345–9354.

(11) (a) Hazuda, D. J.; Felock, P.; Witmer, M.; Wolfe, A.; Stillmock, K.; Grobler, J. A.; Espeseth, A.; Gabryelski, L.; Schleif, W.; Blau, C.; Miller, M. D. Inhibitors of Strand Transfer That Prevent Integration and Inhibit HIV-1 Replication in Cells. *Science* **2000**, *28*, 646–650. (b) Long, Y.; Jiang, X.; Dayam, R.; Sanchez, T.; Shoemaker, R.; Sei, S.; Neamati, N. Rational Design and Synthesis of Novel Dimeric Diketoacid-Containing Inhibitors of HIV-1 Integrase: Implication for Binding to Two Metal Ions on the Active Site of Integrase. *J. Med. Chem.* **2004**, *47*, 2561–2573. (c) Bacchi, A.; Carcelli, M.; Compari, C.; Fiscaro, E.; Pala, N.; Rispoli, G.; Rogolino, D.; Sanchez, T. W.; Sechi, M.; Neamati, N. HIV-1 IN Strand Transfer Chelating Inhibitors: A Focus on Metal Binding. *Mol. Pharmaceutics* **2011**, *8*, 507–519. (d) Bacchi, A.; Carcelli, M.; Compari, C.; Fiscaro, E.; Pala, N.; Rispoli, G.; Rogolino, D.; Sanchez, T. W.; Sechi, M.; Sinisi, V.; Neamati, N. Investigating the Role of Metal Chelation in HIV-1 Integrase Strand Transfer Inhibitors. *J. Med. Chem.* **2011**, *54*, 8407–8420.

(12) Johns, B. A.; Kawasuji, T.; Weatherhead, J. G.; Boros, E. E.; Thompson, J. B.; Garvey, E. P.; Foster, S. A.; Jeffery, J. L.; Miller, W. H.; Kurose, N.; Matsumura, K.; Fujiwara, T. Combining Symmetry Elements Results in Potent Naphthyridinone (NTD) HIV-1 Integrase Inhibitors. *Bioorg. Med. Chem. Lett.* **2011**, *21*, 6461–6464 SAR studies around hydroxy-quinoline (OXN), naphthyridine (NAP), and naphthyridinone (NTD) scaffolds are in publication.

(13) (a) Krishnan, L.; Li, X.; Naraharsetty, H. L.; Hare, S.; Cherepanov, P.; Engelman, A. Structure-Based Modeling of the Functional HIV-1 Intasome and Its Inhibition. *Proc. Natl. Acad. Sci. U. S. A.* **2010**, *107*, 15910–15915. (b) Hare, S.; Gupta, S. S.; Valkov, E.; Engelman, A.; Cherepanov, P. Retroviral Intasome Assembly and Inhibition of DNA Strand Transfer. *Nature* **2010**, *464*, 232–236. (c) Hare, S.; Vos, A. M.; Clayton, R. F.; Thuring, J. W.; Cummings, M. D.; Cherepanov, P. Molecular Mechanisms of Retroviral Integrase Inhibition and the Evolution of Viral Resistance. *Proc. Natl. Acad. Sci. U. S. A.* **2010**, *107*, 20057–20062. (d) Hare, S.; Smith, S. J.; Metifiot, M.; Jaxa-Chamiec, A.; Pommier, Y.; Hughes, S. H.; Cherepanov, P. Structural and Functional Analyses of the Second-Generation Integrase Strand Transfer Inhibitor Dolutegravir (S/GSK1349572). *Mol. Pharmacol.* **2011**, *80*, 565–572.

(14) Kawasuji, T.; Fuji, M.; Yoshinaga, T.; Sato, A.; Fujiwara, T.; Kiyama, R. 3-Hydroxy-1,5-dihydro-pyrrol-2-one Derivatives as Advanced Inhibitors of HIV Integrase. *Bioorg. Med. Chem.* **2007**, *15*, 5487–5492.

(15) Kobayashi, M.; Yoshinaga, T.; Seki, T.; Wakasa-Morimoto, C.; Brown, K. W.; Ferris, R.; Foster, S. A.; Hazen, R. J.; Miki, S.; Suyama-Kagitani, A.; Kawachi-Miki, S.; Taishi, T.; Kawasuji, T.; Johns, A. B.; Underwood, R. M.; Garvey, P. E.; Sato, A.; Fujiwara, T. In Vitro Antiretroviral Properties of S/GSK1349572, a Next-Generation HIV Integrase Inhibitor. *Antimicrob. Agents Chemother.* **2011**, *55*, 813–821.

(16) Further scaffold development and SAR will be reported in future publications.

(17) Isaka, Y.; Sato, A.; Miki, S.; Kawauchi, S.; Sakaida, H.; Hori, T.; Uchiyama, T.; Adachi, A.; Hayami, M.; Fujiwara, T.; Yoshie, O. Small Amino Acid Changes in the V3 Loop of Human Immunodeficiency Virus Type 2 Determines the Coreceptor Usage for CXCR4 and CCR5. *Virology* **1999**, *264*, 237–243.

(18) Harada, S.; Koyanagi, Y.; Yamamoto, N. Infection of HTLV-III/LAV in HTLV-I-Carrying Cells MT-2 and MT-4 and Application in a Plaque Assay. *Science* **1985**, *229*, 563–566.